A novel 'bottom-up' synthesis of few- and multi-layer graphene platelets with partial oxidation via cavitation

Richard J. Price,*[a] Paul I. Ladislaus,[b] Graham C. Smith, [a] and Trevor J. Davies [a, c]

* Corresponding author: r.price@chester.ac.uk

[a] Faculty of Science and Engineering, Department of Natural Sciences, University of Chester, Thornton Science Park, Pool Lane, Ince, Chester CH2 4NU, UK.

[b] Thomas Swan Ltd., Rotary Way, Consett, County Durham, DH8 7ND, UK.

[c] now at Inovyn ChlorVinyls Limited, South Parade, PO Box 9, Runcorn, WA7 4JE, UKA

Abstract

The transient cavitation of diaromatic components such as 1-methylnaphthalene has been used to produce graphene platelets in a 'bottom-up' synthesis via the high temperature (> 5000 K) conditions that are generated inside collapsing bubbles. Acoustic cavitation produced yields of 5.7 x 10^{-11} kgJ^{-1} at a production rate of 2.2 x10^{-9} kgs^{-1}. This can be improved by generating cavitation hydrodynamically, thus making commercial scale production viable. Hydrodynamic cavitation produced platelets with larger lateral dimensions (≥ 2 μm) than those formed by acoustic cavitation (10–200 nm). The partially oxidised nature of the platelets enables their covalent chemical functionalization, which was achieved by combining suitable molecules in the reaction medium to affect a *one-pot* formation and functionalization of graphene.

Keywords: cavitation, graphene, hydrodynamic, functionalization, synthesis, ultrasound

1. Introduction

Graphene in its pristine form is a two-dimensional single layer of hexagonally arranged carbon atoms. It has been shown to have exceptional electrical [1] and thermal conductivity [2], high mechanical strength [3] and a large surface area [4]. Sheets of the material are flexible [5], impermeable to gases [6] and relatively transparent [7]. This interesting set of properties has led to a broad range of potential applications including its use in electronic devices, energy storage materials, polymer nanocomposites, conductive inks and sensors: a road map for graphene-based disruptive technologies has been the subject of recent review [8].

One of the biggest challenges to the successful future application of graphene in new devices is the need to develop commercially viable production methods: again current

approaches have been comprehensively reviewed [8,9]. Successful routes to graphene production require cost-effective scalability but typically involve trade-offs between the ease of production and final material quality. A good deal of the focus has been on 'top-down' methods that involve breaking stacked layers of graphite apart to yield graphene sheets. Dry exfoliation of graphite was first reported by micromechanical cleavage [10] and has subsequently been shown to be possible via anodic bonding [11] and laser induced photoexfoliation [12]. Graphite can also be exfoliated in liquid environments with extraction achieved by electrochemistry [12,13], sonication [14,15] and high shear [16]. All such routes are dependent upon a reliable supply chain of high quality graphite. Other exfoliation-based approaches include the conversion of graphite to intercalation compounds or oxidation to graphite oxide, these materials being more prone to delayering [8]. The formation of graphene oxide requires a further reduction step to obtain graphene, however this does not typically go to completion and only reduced forms of graphene oxide have been achieved [17].

'Bottom-up' methods of synthesis from alternative sources of carbon that require high temperatures have also been investigated. Films of graphene can be grown by the thermal decomposition of silicon carbide [18], however substrate removal can present difficulties. Chemical Vapour Deposition (CVD) has been widely used for film production on metal substrates via the pyrolysis of carbon-containing gases [9] but has also been employed without the use of a substrate when material is collected outside of the furnace in a continuous process of production. Examples of such approaches are the microwave-enhanced CVD of ethanol at atmospheric pressure [19,20] and the thermal decomposition of sodium ethoxide in ethanol to produce few-layer graphene via substrate free CVD [21].

Cavitation is the formation and collapse of vapour bubbles in a liquid when it is subjected to rapid changes in pressure. This phenomenon has been actively pursued as a technology for chemical synthesis (sonochemistry) over the last forty years in approaches that have employed cavitation generated by both ultrasound (acoustic cavitation) [22] and in fast flowing liquids (hydrodynamic cavitation) [23]. The vapour bubbles that form in low-pressure regions collapse when subjected to higher pressure, with the implosion generating extremely high-localised temperatures (> 5000 K) and pressures (> 1000 atmosphere) [24,25]. We now report evidence that the cavitation of diaromatic compounds has potential to provide a new route to the production of graphene platelets in both non-functionalized and functionalized forms. As such this represents a distinctively different approach to previously reported gas-phase 'bottom-up' methods of

synthesis in that the reaction take place inside the liquid phase of the reaction medium and does not require a substrate.

2. Materials and methods

2.1 Material preparation

2.1.1 By acoustic cavitation

The compression and rarefaction of ultrasound waves when passed through a liquid can produce bubbles; the formation, growth and collapse of which is known as transient cavitation [22]. The acoustic pressure during rarefaction, if of sufficient magnitude, creates a dynamic tensile stress that causes the liquid to break down leading to the formation of cavities or bubbles. These bubbles – comprised of vapour and dissolved gases – shrink and expand under the influence of the acoustic field. Individual bubbles experience interference from their surroundings and consequently expansion to an unstable size is followed by an implosive collapse during the compression cycle and this produces localised hot spots that are characterised by rapid rates of heating and cooling.

Ultrasound was delivered to 50 mL of hydrocarbon in a jacketed glass beaker at a frequency of 20 kHz with a VCX 750 (750 W) ultra-sonic processor (Sonics Materials Inc., Newtown, CT) and a 13 mm extender horn. Circulating cold water (10 °C) was used to keep the liquid hydrocarbon well below its flash point. A PTFE lid was used to prevent splashing whilst compressed air or nitrogen was gently blown over the surface of the hydrocarbon to inhibit condensation inside the reaction vessel (Fig. 1). The whole apparatus was housed inside a box to reduce acoustic noise. The ultrasound probe is made of titanium alloy (Ti 6Al-4V) and became tarnished during use due to cavitation erosion. The probe was polished on silicon carbide papers (P400 and P1000) between experiments to maintain a smooth and shiny tip surface. Energy delivery to the probe trip and the reaction rates produced were maintained at consistent levels (relative standard deviations of < 2%) over ca. 20 consecutive experiments, indicating that this cleaning procedure did not have a significant detrimental impact on the probe's dimensions and performance.

{Fig. 1.}

2.1.2 By hydrodynamic cavitation

Hydrodynamic cavitation is the process of generating vapour bubbles in a flowing liquid followed by their subsequent implosion caused by a decrease and then an increase of pressure [23]. For example, constricting the flow of a liquid with a throttling valve, orifice plate or venturi

can produce such pressure changes. When the liquid passes through the constriction there is an increase in velocity of flow accompanied by a drop in pressure. If the pressure around the *vena contracta* drops below a critical threshold (typically the vapour pressure of the liquid at the operating temperature) then vapourisation occurs and cavitation bubbles are produced.

Experiments were conducted in a Panda Plus 2000 homogenizer (GEA Niro Soavi, Parma, Italy) previously used to generate high shear rates for the exfoliation of graphene from graphite [26]. The technology was originally developed to create stable emulsions or dispersions by forcing a fluid through a conduit onto an impact head that can be moved to create an adjustable gap (1–500 μm) (Fig. 2). By treating diaromatic components in the apparatus with a high upstream pressure (P_u = 600–1500 bar) and a low downstream pressure (P_d = 30 bar) it is possible to generate a fast moving cavitating flow and therefore utilise the homogeniser as a hydrodynamic reactor [27].

{Fig. 2.}

2.2 Characterisation details

2.2.1 TEM

Dispersions were filtered onto a holey carbon film suspended on 300 mesh copper TEM grids (Agar Scientific Ltd, Stansted UK). Imaging was performed in transmission mode using a Phillips CM20 TEM (Phillips, now FEI/Thermo-Fischer, Eindhoven) at 200 kV beam energy.

2.2.2 SEM and EDX

Analysis on powder samples was carried out using a Leo (now Zeiss) 1455VP SEM at 20 kV beam energy with 30 pA beam current. EDX analysis was performed using an Oxford Instruments X-Act ultra-thin window EDX detector with Oxford INCA acquisition and processing software. Images were acquired of a typical area at x500 and x5000 magnification.

2.2.3 Raman spectroscopy

Raman spectra were recorded using a Renishaw InVia Raman Microscope (Renishaw plc., Wolton-upon-Edge, UK) with a 532 nm laser and 2400 l/mm (vis) grating and a Horiba Jobn-Yvon Xplora Plus Raman Microscope using a 532 nm laser.

2.2.4 XPS

XPS studies were performed using a purpose-built ultra-high vacuum system equipped with a Specs PHOIBOS 150 electron energy analyser and Specs FOCUS 500 monochromated Al K$_\alpha$ X-ray source (Specs GmbH, Berlin, Germany). Samples were prepared for analysis by filtering

dispersions through unsupported alumina membranes with a 0.2 μm pore size followed by washing with *iso*-propanol and vacuum drying. Survey and narrow scans were acquired over the binding energy range between 0 and 1100 eV using a pass energy of 50 eV and high resolution scans were made over individual photoelectron lines using a pass energy of 15 eV. Data processing and curve fitting were carried out using CasaXPS software v2.3.16, with quantification carried out using Scofield cross-sections corrected for the energy dependence of the analyser transmission and the effective electron attenuation lengths.

2.2.5 Laser particle counter

Particle analysis was carried out using a Spectrex LPC-2200 laser particle counter (Spectrex Corporation, Redwood City, CA), which makes measurements based on the principle of near-angle light scattering. Samples were gently swirled before being left to stand to allow any air bubbles settle. Number density counts were based on an average of ten consecutive measurements. When the number concentration (N) is > 1000 cm^{-3} there is a risk of overlap between particles in the third dimension (i.e. closer to or further from the detector), which may lead to two or more small particles being counted as a single large particle. Sample dilution with chromatography grade *n*-heptane that has a low background particle count (< 20 cm^{-3}) was used to prevent this artefact from occurring. Hydrocarbons were pre-filtered (1.0 μm PTFE Acrodisc membrane ex Sigma Aldrich) before treatment with ultrasound. The background count for all solvents was < 50 cm^{-3}. Individual platelets with lateral dimensions < 1 μm are not detected by the technique, which counts particles in the 1–100 μm range. When platelets agglomerate to ≥ 1 μm sized particles they become countable.

2.2.6 UV-vis spectroscopy

UV-vis spectra were recorded using a UV-1699PC VWR spectrophotometer (VWR International, Radnor, PA). The absorbance of light at 660 nm was used to monitor the reaction rate of graphene platelet production and the stability of the dispersions produced.

2.2.7 AFM

Samples for AFM analysis were produced by drop casting (10 μL) of dispersed platelets (*ca.* 0.1 mg mL^{-1}) in N-methyl-2-pyrollidone (NMP) onto clean Si(111) wafers (Agar Scientific Ltd, Stansted UK) held above the boiling point of the solvent. Freshly cut Si(111) wafers were prepared by sonication in acetone, deionised water and *iso*-propanol before drying. Samples were imaged in Tapping Mode using an NT-MDT Solver Next AFM (NT-MDT, Moscow) with Si_3N_4 tips.

3. Results and discussion

3.1. Acoustic cavitation

1-Methylnaphthalene (1-MN, b.p. 243 °C and m.p. -22 °C) when treated with 20 kHz ultrasound changed from a pale-yellow hydrocarbon into a black dispersion within a few minutes (Fig. 3). The processor's in-built meter measured the power delivery to the ultrasound probe at 72 W. Calorimetric measurements (described in Section A, SI) were used to determine a transfer of 39 W into the reaction medium (η = 53%). This equates to a power intensity of 30 Wcm^{-2} at the 1.27 cm^2 probe tip, which is sufficient to induce transient cavitation. Upon completion the laser particle counter was used to characterise the number density (N) of ≥ 1 μm particles present. Typically 4 x 10^6 cm^{-3} were found after a treatment of 600 kJ and a running time of 137 minutes (Section B in SI). This count increased significantly to 15 x 10^6 cm^{-3} due to platelet agglomeration when the dispersion was left to stand over an extended period (>10 days). Dispersions were not stable and floc formation followed by sedimentation typically occurred within a day of standing.

{Fig. 3}

The sediment was removed by centrifugation (3500 rmin^{-1} for 20 minutes) followed by filtration through a 0.7 μm Whatman glass microfiber filter, Grade GF/F. Addition of *n*-heptane to the filtrate followed by further centrifugation and a second filtration enabled a gravimetric analysis of all the material produced during cavitation (Fig. 4), from which a cavitational yield (*CY*) of 5.7 x 10^{-11} kgJ^{-1} and a production rate (*PR*) of 2.2 x 10^{-9} kgs^{-1} are calculated.

{Fig. 4}

TEM analysis showed that thin flakes with lateral dimensions of 10–200 nm were produced (Fig. 5a). These flakes are sufficiently small that collisions produced by the shear forces generated during cavitation are minor compared to thermally induced collisions that are independent of platelet size (Peclet number, P_e, < 1). The laser particle counter cannot detect small platelets but the thermally driven collision of platelets after cavitation resulted in agglomeration and an increase in the number density of ≥ 1 μm particles (Fig. 5b). These larger particles then formed flocs that undergo sedimentation.

{Fig. 5}

Transient cavitation involves the formation, growth and collapse of vapour bubbles. The maximum temperature (T_{max}) developed during the adiabatic implosion can be determined by

$$T_{max} = T_0 \left[P_m (\gamma - 1)/P_v\right] \tag{1}$$

where T_0 is the ambient temperature, γ is the heat capacity ratio, P_m is the pressure in the liquid at the moment of bubble collapse and P_v is the vapour pressure of the liquid [28]. The low vapour

pressure of 1-MN (24 Nm^{-2} at the equilibrated temperature of 313 K developed during cavitation) resulted in high temperatures that produced homolytic fission of C–H bonds and rapid rates of graphitisation. The reaction slowed or switched off when more volatile mono-aromatics were used (e.g. toluene, b.p. 111 °C, $T_{max}[\mathbf{1-MN}]/T_{max}[\textbf{toluene}] \sim \mathbf{200}$) but was enhanced by dissolving solid diaromatic compounds with fused (naphthalene, b.p. 218 °C, m.p. 80 °C) or linked rings (biphenyl, b.p. 255 °C, m.p. 69 °C) into 1-MN (Fig. 6). The reaction of diaromatic components can proceed as a cyclodehydrogenation and a combination of *peri-* and *cata*-condensations allows two-dimensional sheets to grow (Scheme 1) [29–31].

{Fig. 6}

{Scheme 1}

Degassing of solvents occurs during cavitation but this is partial [32] and does not remove all the dissolved air that is typically present in a hydrocarbon (~100 mg/L) [33]. Consequently bubbles contained a mixture of hydrocarbon vapour and residual air, giving rise to the formation of platelets that were partially oxidised (see C 1s XPS and Raman spectra in Fig. 7). XPS data indicated material with an atomic C/O ratio of 10, similar in character to reduced graphene oxide (rGO) [17,34]. Sparging the reaction mixture with nitrogen before commencing cavitation produced less oxidised platelets (atomic C/O ratio of 15) and dispersions with increased stability (Fig. 8).

{Fig. 7}

{Fig. 8}

3.2 Functionalization

A variety of reactions (electrophilic substitution, nucleophilic substitution, condensation and addition) have been reported for graphene oxide (GO) and rGO which allow the production of functionalized forms of graphene [35,36]. The partially oxidised nature of the platelets produced by cavitation enables such covalent modifications to be carried out as a *one-pot* synthesis by including suitable molecules in the diaromatic reaction medium. This has been demonstrated with alkyl and phenyl molecules containing –OH, –NH$_2$ and –CO$_2$H groups that produce a change in dispersion stability (Section C in SI). This was most successfully achieved with alkyl amines, which are known to enable the attachment of alkyl ligands to platelets via the nucleophilic ring opening of epoxide groups and condensation reactions with carboxylic acid groups [37]. For example, introducing octylamine in to the reaction mixture (ϕ = 0.1) resulted in the formation of

a dispersion with a particle number density (N) of 0.3 x 10^6 cm^{-3} and an extended stability time (A/A_0 = 0.5 > 100 days).

Cloudy macroemulsions were produced when some functionalising molecules (water, hydrogen peroxide, formic acid) were combined and shaken with 1-MN. This initial lack of solubility was followed by the formation during cavitation of optically transparent, kinetically stable nanoemulsions. Reactions appeared to still take place, producing more polar platelets (Section C, Table S.3 in SI).

The ability to react molecules with boiling points that are higher than that of 1-MN (Section D in SI) indicates that the functionalizing chemistry takes place in the hot liquid zone that forms around the collapsing bubbles (*secondary sonochemistry*) after the partially oxidised platelets are formed in the vapour phase inside the cavitation bubbles (*primary sonochemistry*) [24].

3.3 Scale up

Scale up is not easily achieved with ultrasound cavitation because the technique typically shows reaction rates that initially increase but then limit and eventually decrease with increasing power input. This is due to the number of cavities becoming so high in the vicinity of the probe tip that the transfer of ultrasound energy into the reaction medium is attenuated [38]. Hydrodynamic cavitation that is produced by the decrease and subsequent increase in local pressure in flowing liquids offers a more attractive means of achieving higher production rates. The pressure drop as the fluid flows around the impact head in the reactor generates cavitation and in hydrodynamic systems this phenomenon is often characterised by a non-dimensional cavitation number (C_v) [27]

$$C_v = (P_r - P_v)/\left(\frac{1}{2}\rho v^2\right) \tag{2}$$

where P_r is the pressure at a reference point in the flow, P_v is the vapour pressure of the liquid, v is the fluid velocity at the reference point and ρ is the density of the fluid. At large C_v the flow is single-phase but when the flow is sufficiently fast and P_r becomes close to P_v (i.e. when C_v decreases) cavitation begins to occur. A critical cavitation number ($C_{v(cr)}$) is used to define this point of incipient cavitation. As C_v drops below $C_{v(cr)}$ the number of cavitation events increases.

An alternative cavitation number (CN) that has been used for the delivery of hydrocarbon fuels by injectors in diesel and gasoline engines is

$$CN = (P_u - P_d)/(P_d - P_v) \tag{3}$$

where P_u is the pressure upstream and P_d is the recovered pressure downstream of the point of cavitation. It is known that critical numbers ($CN_{(cr)}$) for fuel injectors fall in the range of 0.5–10 [39] and that similar values also apply for hydrocarbons in the middle distillate boiling range when cavitation occurs in immersed jet shear flows ($CN_{(cr)}$ of 5–20) [40]. The conditions used and the samples prepared in the homogenizer are given in Table 1. The cavitation number increases as the velocity of the flow becomes faster and CN was sufficiently high in all cases (19–49) to produce cavitation in fast moving flows (>300 ms^{-1}) of 1-MN (Table 1), which resulted in the rapid formation of black dispersions. The atomic C/O ratio of thin films (XPS) and powder samples (SEM-EDX) is consistent with partially oxidised platelets but shows some variation with P_u (Table 1). When octylamine was employed in the reaction mixture the atomic C/O ratio became closer to values measured for graphene flakes produced by the exfoliation of graphite in the same reactor (Table 1).

{Table 1}

TEM analysis reveals that hydrodynamic cavitation produced larger platelets with lateral dimensions ≥ 2 μm (Fig. 9 a-c) and thicknesses of 5–30 nm, with evidence of sheet folding (Section E in SI). These are similar to the graphene flakes produced in the same reactor when it was used to generate graphene via shear-induced exfoliation of graphite in water (Fig. 9 d and Section E in SI).

{Fig. 9}

A cavitation bubble of 100 μm diameter contains sufficient carbon to theoretically grow a 30 μm x 30 μm single layer graphene sheet, however it is unlikely that all of the carbon present undergoes transformation into a graphene platelet. The pressures employed in the hydrodynamic reactor (P_u = 600–1500 bar) were higher than those used during acoustic cavitation ($\square_A$ < 10 bar) and this would be anticipated to result in larger bubble formation [41]. Larger bubbles contain more moles of 1-MN, which has the apparent consequence of the formation of platelets with larger lateral dimensions.

The XPS C 1s for platelets ex 1-MN w/ octylamine showed sp^2 carbon-carbon bonds similar to exfoliated graphene but with additional features at higher energy which are difficult to assign but are thought to be due to bonds established between platelet carbon and the alkyl amine functionalising molecule (Fig. 10). Platelet colouration and UV-vis spectra were similar to exfoliated graphene, whereas the smaller platelets produced by ultrasound cavitation had a brown colouration and somewhat different optical transmission spectra (Section F in SI).

{Fig. 10}

Hydrodynamic reactors are known to give improved cavitation yields compared to acoustic reactors (typically by at least an order of magnitude) [14] and the flow of liquid away from the point at which bubbles are formed means that physical scaling can be employed to allow higher power inputs. For example the technology employed in the Panda Plus 2000 homogenizer is scalable and equipment is commercially available that spans volumetric flow rates from 10's lh^{-1} through to 10's m^3h^{-1} [42]. The level of power input (> 500 kW) that would enable production rates > 1 kgh^{-1} is therefore in principle achievable.

4. Conclusions

A scalable method for the synthesis of graphene platelets via the transient cavitation of diaromatic components has been demonstrated. Collapsing bubbles filled with diaromatic vapour produce localised points of extremely high temperature that are sufficient to drive cyclodehydrogenation condensation reactions and the formation of two dimensional sheets of hexagonally arranged carbon atoms. If small amounts of oxygen from dissolved air are also present in these bubbles then partially oxidised platelets are formed which are compositionally similar to reduced graphene oxide (rGO). Displacing dissolved oxygen from the reaction medium before commencing cavitation produces purer forms of graphene (higher atomic C/O ratio). However the presence of C–O, C=O and O–C=O groups in partially oxidised platelets allows their covalent modification to be achieved by combining suitable functionalising molecules with the diaromatic component during cavitation. Scalability is achievable by generating cavitation in hydrodynamic reactors, as opposed to systems that rely on bubbles that are generated acoustically. The use of physically larger hydrodynamic reactors with high input energies is realistic and would allow cavitational yields and production rates that are industrially relevant and therefore appropriate for commercial applications.

References

[1]   K.I. Bolotin, K.J. Sikes, Z. Jiang, M. Klima, G. Fudenberg, J. Hone, P. Kim, H.L. Stormer, Ultrahigh electron mobility in suspended graphene, Solid State Commun. 146 (2008) 351–355.

[2]   A.A. Balandin, S. Ghosh, W.Z. Bao, I. Calizo, D. Teweldebrhan, F. Miao, C.N. Lau, Superior thermal conductivity of single-layer graphene, Nano Lett. 8 (2008) 902–907.

[3]   C. Lee, X. Wei, J.W. Kysar, J. Hone, Measurement of the elastic properties and intrinsic strength of monolayer graphene, Science 321 (2008) 385–388.

[4]   L. Zhang, F. Zhang, X. Yang, G. Long, Y. Wu, T. Zhang, K. Leng, Y. Huang, Y. Ma, A. Yu, Y. Chen, Porous 3D graphene-based bulk materials with exceptional high surface area and excellent conductivity for supercapacitors, Sci. Rep. 3 (2013) 1408.

[5]   K.S. Kim, Y. Zhao, H. Jang, S.Y. Lee, J.M. Kim, K.S. Kim, J.H. Ahn, P. Kim, J.Y. Choi, B.H. Hong, Large-scale pattern growth of graphene films for stretchable transparent electrodes, Nature 457 (2009) 706–710.

[6]   J.S. Bunch, S.S. Verbridge, J.S. Alden, A.M. van der Zande, J.M. Parpia, H.G. Craighead, P.L. McEuen, Impermeable atomic membranes from graphene sheets, Nano Lett. 8 (2008) 2458–2462.

[7]   R.R. Nair, P. Blake, A.N. Grigorenko, K.S. Novoselov, T.J. Booth, T. Stauber, N.M.R. Peres, A.K. Geim, Fine structure constant defines visual transparency of graphene, Science 320 (2008) 1308–1308.

[8]   A.C. Ferrari et al., Science and technology roadmap for graphene related two-dimensional crystals and hybrid systems, Nanoscale 7 (2015) 4598–4810.

[9]   R.S. Edwards, K.C. Coleman, Graphene synthesis: relationship to application, Nanoscale 5 (2013) 38–51.

[9]   K.S. Novoselov, A.K. Geim, S.V. Morozov, D. Jiang, Y. Zhang, S.V. Dubonos, I.V. Grigorieva, A.A. Firsov, Electric field effect in atomically thin carbon films, Science 306 (2004) 666–669.

[10]   T. Moldt, A. Eckmann, P. Klar, S.V. Morozov, A.A. Zhukov, K.S. Novoselov, C. Casiraghi, High-yield production and transfer of graphene flakes obtained by anodic bonding, ACS Nano 5 (2011) 7700–7706.

[11] S. Dhar, A. Roy Barman, G.X. Ni, X. Wang, X.F. Xu, Y. Zheng, S. Tripathy, Ariando, A. Rusydi, K.P. Loh, M. Rubhausen, A. H. Castro Neto, B. Őzyilmaz, T. Venkatesan, A new route to graphene layers by selective laser ablation, AIP Adv. 1 (2011) 022109.

[12] G. Wang, B. Wang, J. Park, Y. Wang, B. Sun, J. Yao, Highly efficient and large-scale synthesis of graphene by electrolytic exfoliation, Carbon 47 (2009) 3242–3246.

[13] C.-Y. Su, A.-Y. Lu, Y. Xu, F.-R. Chen, A.N. Khlobystov, L.-J. Li, High quality thin graphene films from fast electrochemical exfoliation, ACS Nano 5 (2011) 2332–2339.

[14] P. Blake, P.D. Brimicombe, R.R. Nair, T.J. Booth, D. Jiang, F. Schedin, L.A. Ponomarenko, S.V. Morozov, H.F. Gleeson, E.W. Hill, A.K. Geim, K.S. Novoselov, Graphene-based liquid crystal device, Nano Lett. 8 (2008) 1704–1708.

[15] Y. Hernandez, V. Nicolosi, M. Lotya, F.M. Blighe, Z. Sun, S. De, I.T. McGovern, B. Holland, M. Byrne, Y.K. Gun'ko, J.J. Boland, P. Niraj, G. Duesberg, S. Krishnamurthy, R. Goodhue, J. Hutchison, V. Scardaci, A.C. Ferrari, J.N. Coleman, High-yield production of graphene by liquid-phase exfoliation of graphite, Nat. Nanotechnol. 3 (2008) 563–568.

[16] K.R. Paton et al., Scalable production of large quantities of defect-free few-layer graphene by shear exfoliation in liquids, Nat. Mater. 13 (2014) 624–630.

[17] D.R. Dreyer, S. Park, C.W. Bielawski, R.S. Ruoff, The chemistry of graphene oxide, Chem. Soc. Rev. 39 (2010) 228–240.

[18] K.V. Emtsev, A. Bostwick, K. Horn, J. Jobst, G.L. Kellogg, L. Ley, J.L. McChesney, T. Ohta, S.A. Reshanov, J. Rohrl, E. Rotenberg, A.K. Schmid, D. Waldmann, H.B. Weber, T. Seyller, Towards wafer-size graphene layers by atmospheric pressure graphitization of silicon carbide, Nat. Mater. 8 (2009) 203–207.

[19] A. Dato, V. Radmilovic, Z. Lee, J. Phillips, M. Frenklach, Substrate-free gas-phase synthesis of graphene sheets, Nano Lett. 8 (2008) 2012–2016.

[20] A. Dato, M. Frenklach, Substrate-free microwave synthesis of graphene: experimental conditions and hydrocarbon precursors, New J. Phys. 12 (2010) 125013.

[21] C.R. Herron, K.S. Coleman, R. . Edwards, B.G. Mendis, Simple and scalable route for the 'bottom-up' synthesis of few-layer graphene and thin films, J. Mater. Chem. 21 (2011) 3378–3383.

[22] T. J. Mason, J. P. Lorimer, Applied Sonochemistry: The Use of Power Ultrasound in Chemistry and Processing, first ed., Wiley-VCH Verlag GmbH, Weinham, 2002.

[23] P.R. Gogate, A.B. Pandit, A review and assessment of hydrodynamic cavitation as a technology for the future, Ultrason. Sonochem. 12 (2005) 21–27.

[24] H. Xu, B. W. Zeiger, K.S. Suslick, Sonochemical synthesis of nanomaterials, Chem. Soc. Rev. 42 (2013) 2555–2567.

[25] K. S. Suslick, J. J. Gawienowski, P. F. Schubert, H. H. Wang, Alkane sonochemistry, J. Phys. Chem. 87 (1983) 2299–2301.

[26] UK Patent GB2545060B, Apparatus and method for bulk production of atomically thin 2-dimensional materials including graphene, 2018.

[27] P.M. Kanthale, P.R. Gogate, A.B. Pandit, A.M. Wilhelm, Dynamics of cavitational bubbles and design of a hydrodynamic cavitational reactor: cluster approach, Ultrason. Sonochem. 12 (2005) 441–452.

[28] Mason, Applied Sonochemistry, p54.

[29] M. Murakami, Morphology and polymerization mechanism of one-dimensional graphite polymer, poly-peri-naphthalene, Synth. Met. 18 (1987) 531–536.

[30] H. Kamo, M. Yudasaka, S. Kurita, T. Matsui, R. Kikuchi, Y. Ohki, S. Yoshimura, Formation of poly-peri-naphthalene thin films by chemical vapour deposition, Synth. Met. 68 (1994) 61–63.

[31] M. Treier, C.A. Pignedoli, T. Laino, R. Rieger, K. Mullen, D. Passerone, R. Fasel, Surface-assisted cyclodehydrogenation provides a synthetic route towards easily processable and chemically tailored nanographenes, Nat. Chem. 3 (2011) 61–67.

[32] T. Vencel, J. Donovalova, A. Gaplovsky, T. Kimura, S. Toma, Oxygen exclusion from organic solvents using ultrasound and comparison with other common techniques used in photochemical experiments, Chem. Pap. 59 (2005) 271–274.

[33] J.A. Schetz, A.E. Fuhs (Eds.), Handbook of Fluid Dynamics and Fluid Machinery: Fundamentals of Fluid Dynamics, Volume I, Wiley & Sons Inc., Chichester, 1996, pp161–162.

[34] K. Krishnamoorthy, M. Veerapandian, K. Yun, S.-J. Kim, The chemical and structural analysis of graphene oxide with different degrees of oxidation, Carbon 53 (2013) 38–49.

[35] D.W. Johnson, B.P. Dobson, K.S. Coleman, A manufacturing perspective on graphene dispersions, Curr. Opin. Colloid Interface Sci. 20 (2015) 367–382.

[36] T. Kuila, S. Bose, A.K. Mishra, P. Khanra, N.H. Kim, J.H. Lee, Chemical functionalization of graphene and its applications, Prog. Mater. Sci. 57 (2012) 1061–1105.

[37] J. Jang, V.H. Pham, S.H. Hur, J.S. Chung, Dispersibility of reduced alkylamine-functionalized graphene oxides in organic solvents, J. Colloid Interf. Sci. 424 (2014) 62–66.

[38] Mason, Applied sonochemistry, p77

[39] P.G. Aleiferis, J. Serras-Pereira, A. Augoye, T.J. Davies, R.F. Cracknell, D. Richardson, Effect of fuel temperature on in-nozzle cavitation and spray formation of liquid hydrocarbons and alcohols from a real-size optical injector for direct-injection spark-ignition engines, Int. J. Heat Mass Tranf. 53 (2010) 4588–4606.

[40] R. D. Lockett, N. Ndamuso, R. Price, Cavitation inception in immersed jet shear flows, J. Phys. Conf. Ser. 656 (2015) 012090.

[41] Mason, Applied sonochemistry, p59.

[42] GEA Group AG, Laboratory and Industrial Homogenizers, https://www.gea.com/en/productgroups/homogenizers/index.jsp, 2018 (accessed 1 December 2018).

Table 1 Conditions employed for the formation of graphene platelets in the hydrodynamic reactor via the cavitation of 1-methylnaphthalene w/ and w/o octylamine present. [a]Estimates of the Bernoulli velocity. [b]Platelets ex 1-MN w/o octylamine. [c]Platelets ex 1-MN w/ octylamine (ϕ = 0.1). Atomic C/O (XPS) = 43 and atomic C/O (SEM-EDX) = 85 for graphene platelets produced by the exfoliation of graphite.

P_u	P_d	CN	v[a]	Platelet composition	
(bar)	(bar)	(-)	(ms^{-1})	atomic C/O (XPS)	atomic C/O (SEM-EDX)
600	30	19	337	6[b]	4[b]
1000	30	32	440	13[b], 24[c]	22[b], 73[c]
1500	30	49	542	8[b]	15[b]

cata-condensation

peri-condensation
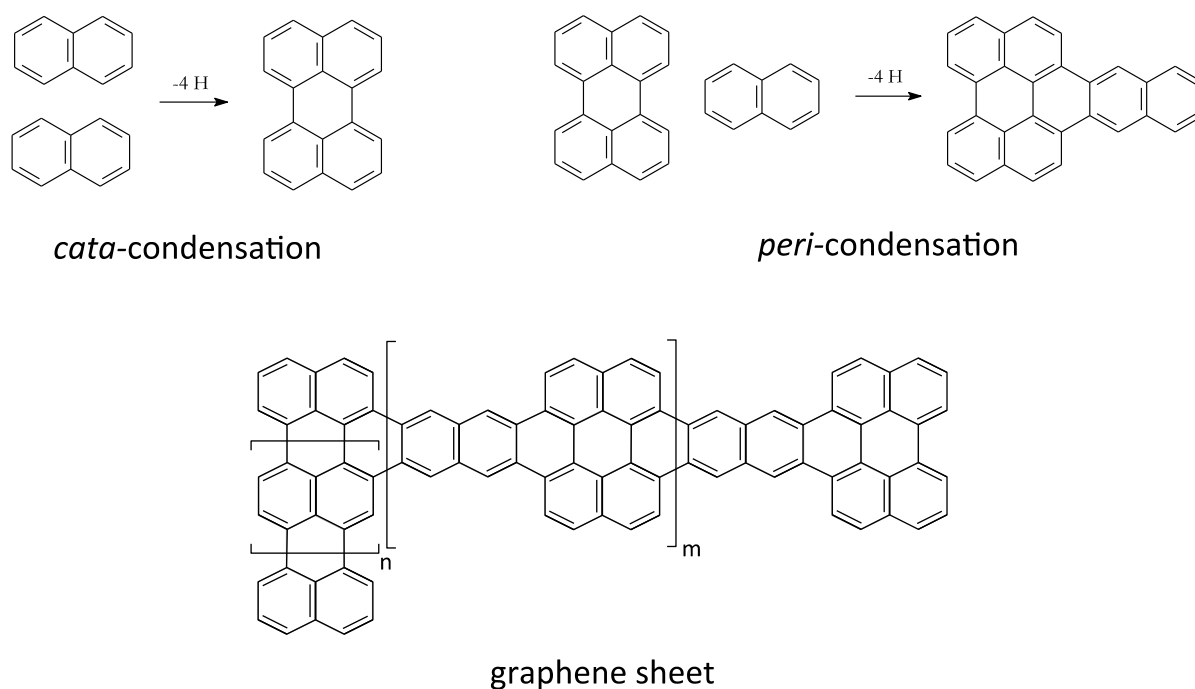
graphene sheet

Scheme 1. Formation of graphene sheets via cyclodehydrogenation reactions.

List of Figures

Fig. 1. Schematic of experimental apparatus used for the treatment of diaromatic compounds with ultrasound.

Fig. 2. Schematic of homogenizer used as a hydrodynamic reactor for the cavitation of diaromatic compounds.

Fig. 3. 1-Methylnaphthalene (1-MN) before and after treatment with ultrasound.

Fig. 4. Production of platelets in 50 mL of 1-MN as a function of ultrasound treatment time.

Fig. 5. TEM analysis of platelets produced during ultrasound cavitation. (a) From a dispersion of platelets in N-methyl-2-pyrrolidone (NMP). (b) From a dispersions of agglomerated platelets in 1-MN.

Fig. 6. Rate of graphitisation determined by UV-vis absorbance measurements (660 nm) taken at regular intervals during cavitation. The reaction switches off for toluene and the rate increases when naphthalene and biphenyl are dissolved in 1-methylnaphthalene up to their limit of solubility

Fig. 7. Partially oxidised graphene platelets produced by ultrasound cavitation. (a) XPS C 1s spectrum showing evidence for sp^3/sp^2 carbon-carbon bonds (285.0 eV, FWHM = 1.7 eV) and high-energy features consistent with C–O (287.0 eV), C=O (288.6 eV) and O–C=O (290.0 eV) and π-plasmon (low intensity, 291.7 eV). (b) Raman spectrum showing a G band ($\sim$1590 cm^{-1}) that indicates a degree of oxidation and the presence of sp^3 carbon atoms. The D band has higher intensity than in pristine graphene, which can be attributed to defects and disorder at both platelet edge and basal plane. $I_D/I_G \sim$0.83, the FWHM$_G$ of $\sim$87 cm^{-1} and the low intensity 2D band (seen with D+G and 2G overtones) are all consistent with reported behaviour for graphene platelets with a degree of oxidation.[34]

Fig. 8. Dispersion stability in a UV-vis cuvette measured by the absorbance of light at 660 nm. A_0 is the absorbance immediately after the completion of cavitation. Platelets in 1-MN sediment within one day of standing unless a N_2 sparge is used to displace dissolved O_2 from the hydrocarbon before cavitation commences. The addition of NMP (ϕ_{NMP}: = 0.5, $\phi_{1\text{-}MN}$ = 0.5) to a fresh dispersion of cavitated 1-MN can also be used to stabilise dispersions of platelets.

Fig. 9. TEM images of platelets produced by (a-c) hydrodynamic cavitation and (d) by the shear induced exfoliation of graphite. (a) 1-MN and P_u = 600 bar. (b) 1-MN and P_u = 1000 bar. (c) 1-MN w/ octylamine and P_u = 1000 bar.

Fig. 10. XPS C1 s data. (a) Functionalised graphene platelets produced by the hydrodynamic cavitation of 1-MN w/ octylamine (φ = 0.1) (C-C 285.0 eV, FWHM 0.5 eV, atomic C/O ratio 24). (b)

Graphene platelets produced by the exfoliation of graphite (C-C 285.0 eV, FWHM 0.6 eV, atomic C/O ratio 43).
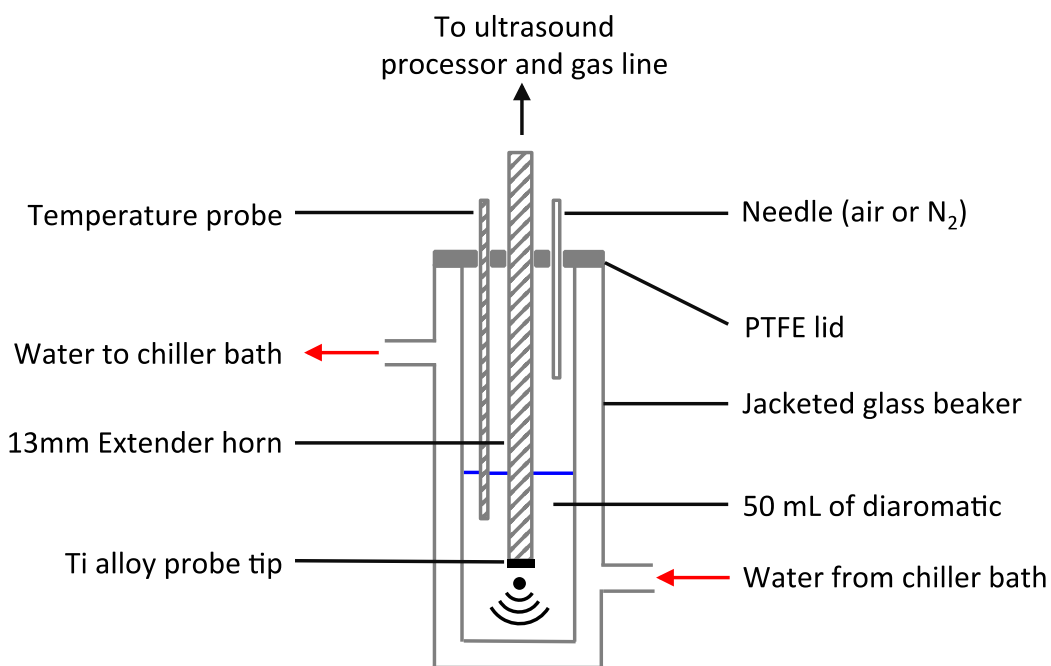
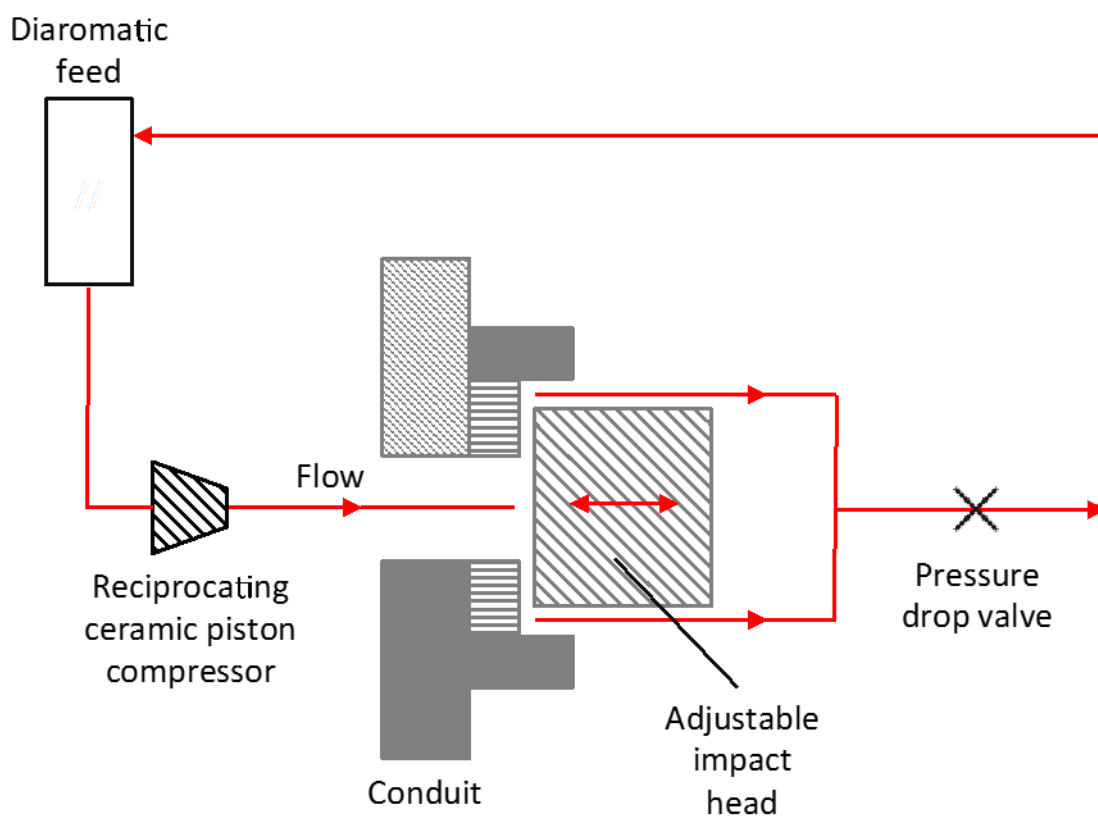**Fig. 1** Schematic of experimental apparatus used for the treatment of diaromatic compounds with ultrasound.

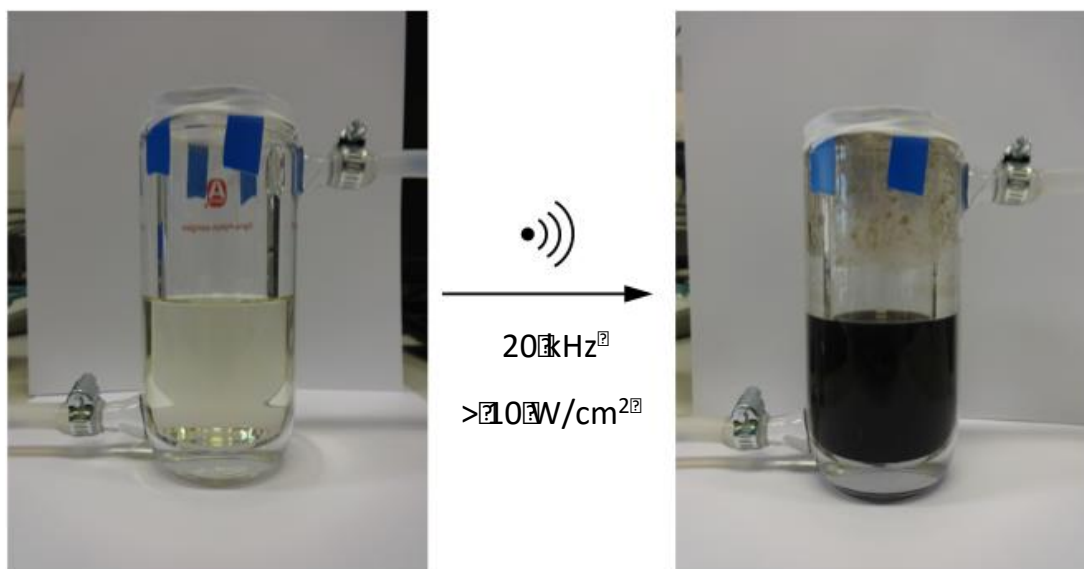**Fig. 2.** Schematic of homogenizer used as a hydrodynamic reactor for the cavitation of diaromatic compounds.

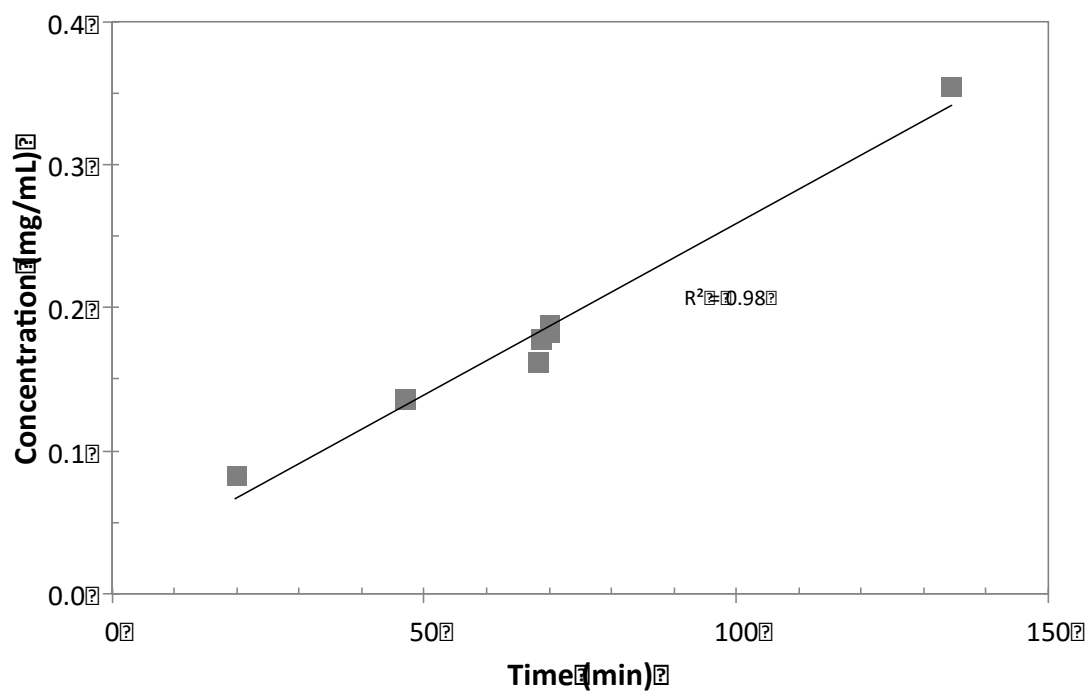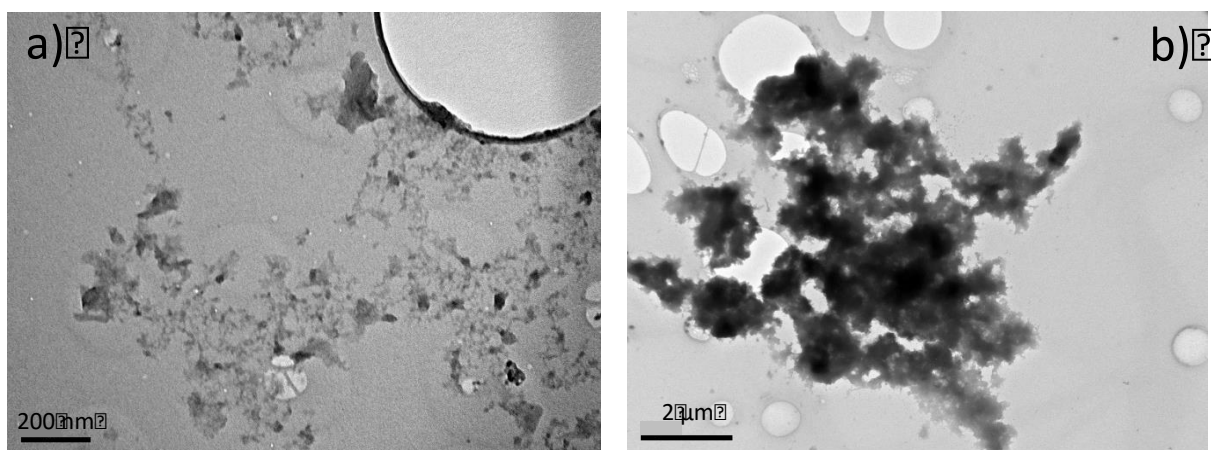**Fig. 3.** 1-Methylnaphthalene (1-MN) before and after treatment with ultrasound.

Fig. 4. Production of platelets in 50 mL of 1-MN as a function of ultrasound treatment time.

Fig. 5. TEM analysis of platelets produced during ultrasound cavitation. (a) From a dispersion of platelets in N-methyl-2-pyrrolidone (NMP). (b) From a dispersions of agglomerated platelets in 1-MN.

Fig. 6. Rate of graphitisation determined by UV-vis absorbance measurements (660 nm) taken at regular intervals during cavitation. The reaction switches off for toluene and the rate increases when naphthalene and biphenyl are dissolved in 1-methylnaphthalene up to their limit of solubility.
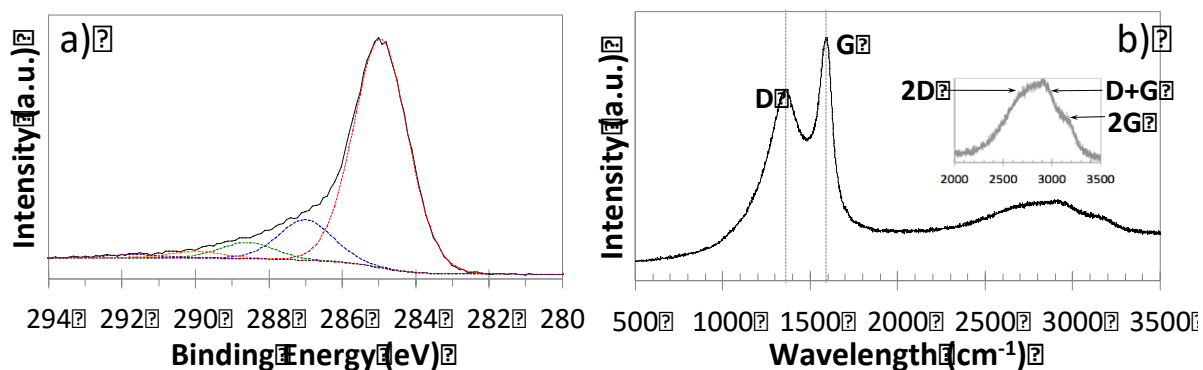
Fig. 7. Partially oxidised graphene platelets produced by ultrasound cavitation. (a) XPS C 1s spectrum showing evidence for sp^3/sp^2 carbon-carbon bonds (285.0 eV, FWHM = 1.7 eV) and high-energy features consistent with C–O (287.0 eV), C=O (288.6 eV) and O–C=O (290.0 eV) and π-plasmon (low intensity, 291.7 eV). (b) Raman spectrum showing a G band (~1590 cm^{-1}) that indicates a degree of oxidation and the presence of sp^3 carbon atoms. The D band has higher intensity than in pristine graphene, which can be attributed to defects and disorder at both platelet edge and basal plane. I_D/I_G ~0.83, the FWHM$_G$ of ~87 cm^{-1} and the low intensity 2D band (seen with D+G and 2G overtones) are all consistent with reported behaviour for graphene platelets with a degree of oxidation.[34]
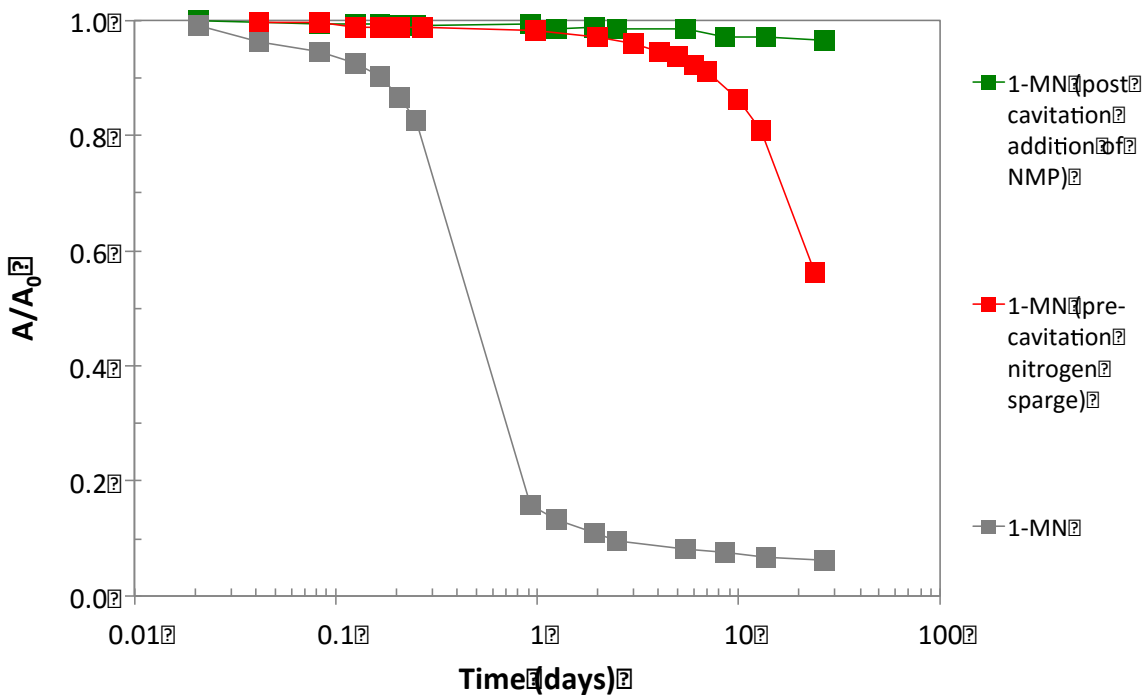
Fig. 8. Dispersion stability in a UV-vis cuvette measured by the absorbance of light at 660 nm. A_0 is the absorbance immediately after the completion of cavitation. Platelets in 1-MN sediment within one day of standing unless a N_2 sparge is used to displace dissolved O_2 from the hydrocarbon before cavitation commences. The addition of NMP (ϕ_{NMP}: = 0.5, $\phi_{1\text{-MN}} = 0.5$) to a fresh dispersion of cavitated 1-MN can also be used to stabilise dispersions of platelets.
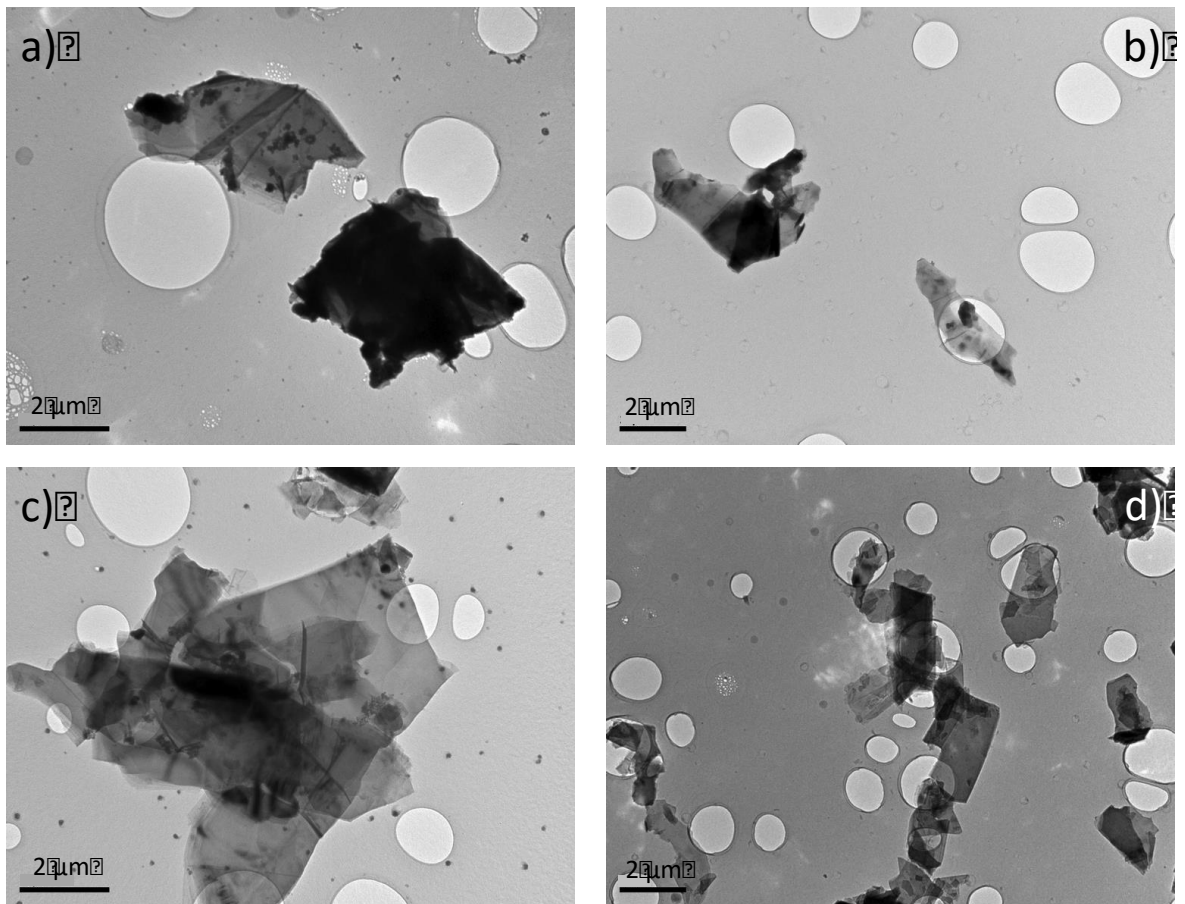
Fig. 9. TEM images of platelets produced by (a-c) hydrodynamic cavitation and (d) by the shear induced exfoliation of graphite. (a) 1-MN and P_u = 600 bar. (b) 1-MN and P_u = 1000 bar. (c) 1-MN w/ octylamine and P_u = 1000 bar.
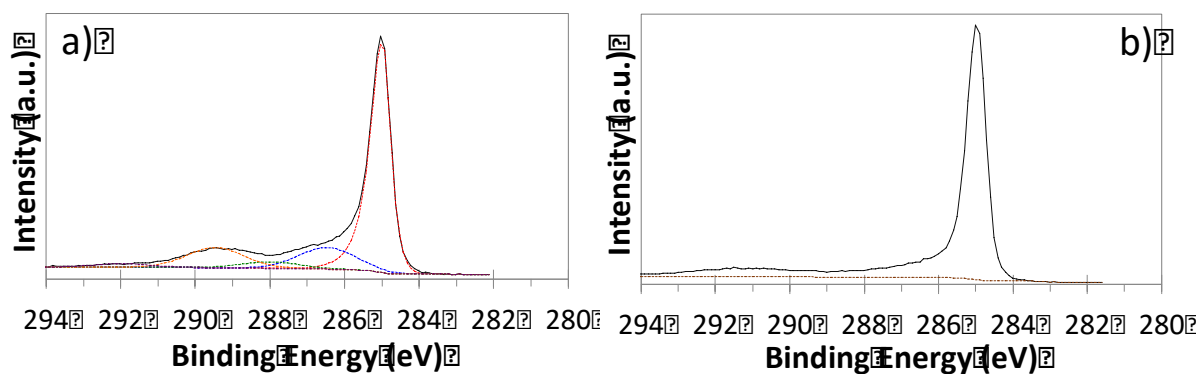
Fig. 10. XPS C1 s data. (a) Functionalised graphene platelets produced by the hydrodynamic cavitation of 1-MN w/ octylamine (ϕ = 0.1) (C-C 285.0 eV, FWHM 0.5 eV, atomic C/O ratio 24). (b) Graphene platelets produced by the exfoliation of graphite (C-C 285.0 eV, FWHM 0.6 eV, atomic C/O ratio 43).